American Mineralogist, Volume 110, pages 1060–1071, 2025

Analcime-wairakite formation during experimental cement-bentonite alteration at 200–300 °C

Amber Zandanel[1,*,†], Kirsten B. Sauer[1], Marlena J. Rock[1], Florie A. Caporuscio[1], Carlos F. Jové-Colón[2], and Edward N. Matteo[2]

[1]Earth and Environmental Sciences Division, Los Alamos National Laboratory, Los Alamos, New Mexico 87545, U.S.A.
[2]Sandia National Laboratories, Albuquerque, New Mexico 87185, U.S.A.

Abstract

Engineered barrier system materials in nuclear waste repositories may undergo hydrothermal alteration in response to groundwater saturation and heating events over their long operational timescales. Hydrothermal interactions between engineered materials (e.g., bentonite buffers, cements, waste canister materials) and the host rock environment may drive alteration processes that affect the advantageous properties of some barrier materials. However, such alteration will also promote the formation of zeolites, hydrothermally formed minerals that may themselves act to isolate radionuclides. Understanding the environmental conditions that control radionuclide-sorbing properties of zeolites, such as Si/Al ratio or Na content, will be valuable for assessing the changing properties of engineered barrier materials in the case of an in situ heating event. Here, we present experimental work characterizing the formation of zeolites during hydrothermal interactions between generic clay and cement barrier materials, with a focus on the analcime-wairakite zeolite series, which has known radionuclide sorption and exchange properties. We present the results of hydrothermal experiments combining uncured ordinary Portland cement powder with steel and Wyoming bentonite in the presence of Opalinus clay and a synthesized Opalinus clay groundwater to simulate water-saturated conditions in an argillaceous rock repository. The experiments were conducted isothermally at 200 or 300 °C for 8 to 24 weeks. In contrast to analogous studies that did not include cement reactants, we observed the formation of analcime-group minerals in all experiments. The addition of cement resulted in lower Si/Al ratios in the zeolites compared to similar studies that did not include cement. The presence of cement as a reactant was interpreted to promote analcime formation at 200 °C. At 300 °C, we observed higher calcium and silica concentrations in the aqueous solutions as well as increased wairakite formation and decreased analcime formation compared to the experiments at 200 °C. These results show a fully realized analcime-wairakite solid solution that falls between Si/Al = 2 (ideal) and a trend of analcime minerals that have increasing Si/Al ratios with increasing Na/(Na+Ca). Our results show predictable relationships between the Si/Al ratio and the analcime-wairakite content under hydrothermal conditions and illustrate that repository material interactions may promote the formation of zeolites in the analcime-wairakite solid-solution series during heating events in the subsurface.

Keywords: Zeolite, hydrothermal experiments, water-rock interaction, analcime, wairakite

Introduction

Deep geologic nuclear waste repository designs must consider complex physical and chemical processes that may result from the interplay between engineered materials and the natural systems of the host rock. Engineered barrier system (EBS) materials are generally selected for their favorable properties in the host environment and ability to contribute to the long-term isolation performance of radionuclides in the subsurface (Pusch 2009; Verstricht 2009; Savage 2011; Sellin and Leupin 2013). However, long-term interactions between EBS components (including bentonite, cements, and waste canister materials) and the host rock environment may drive alteration of both EBS and host rock materials that could affect their radionuclide immobilizing properties over the hundreds or thousands of years of repository lifespan (Hedin 1997; Pusch 2009; Apted and Ahn 2017). This is especially true where such reactions are mediated by a saturating groundwater (Pusch 2009) and/or driven by elevated temperatures (Hardin et al. 2015). In speculative repository designs that consider disposal of dual-purpose canisters (Greenberg et al. 2013; Liljenfeldt et al. 2017), thermomechanical models suggest that EBS materials isolating the spent fuel may reach temperatures exceeding 300 °C (Hardin et al. 2014). The alteration of bentonite, a key EBS component, has been extensively studied to investigate the formation pathways of non-swelling mineral phases (e.g., chlorite, illite) from the degradation of swelling clay minerals (montmorillonite) (Cuadros and Linares 1996; Tinseau et al. 2006; Cheshire et al. 2014; Pusch et al. 2015; Kaufhold and Dohrmann 2016; Tahervand and Jalali 2017; Mills et al. 2023), especially in hydrothermal conditions.

While the negative impacts of hydrothermal alteration on clay minerals are of critical importance to understanding repository functions, another outcome of alteration is the formation of secondary minerals that introduce the potential for radionuclide

* Corresponding author E-mail: azandanel@lanl.gov Orcid https://orcid.org/0000-0002-0940-0751

0003-004X/25/0007–1060$05.00/DOI: https://doi.org/10.2138/am-2024-9490

reaction pathways in EBS materials. A known possibility of EBS alteration is the formation of zeolite minerals, which can act as barriers to radionuclide migration through ion exchange, sorption, and substitution into their structures (as recently reviewed by Jiménez-Reyes et al. 2021). Members of the zeolite mineral group are characterized by [SiO_4] and [AlO_4] tetrahedra that form open channels within their crystal framework (Ames 1960; Smith 1963; Dyer 1988), which host exchangeable cations and can function as molecular sieves (Ames 1960; Davis and Lobo 1992). The properties of natural and synthetic zeolites have valuable applications for immobilizing radioisotopes of strontium (Alby et al. 2018; İnan 2022), cesium (Misaelides 2011; Alby et al. 2018), americium (Mimura et al. 1991; Rajec et al. 1999), uranium (Bhalara et al. 2014; Bakatula et al. 2015), and plutonium (Rajec et al. 1999). In practice, zeolites have been deployed to minimize radionuclide transport from waste sites (Grant et al. 1987; Cantrell 1996; Rabideau et al. 2005) and during remediation efforts, such as those following the Chernobyl disaster (Phillippo et al. 1988; Campbell and Davies 1997).

The zeolite mineral analcime, $Na(AlSi_2O_6)\cdot H_2O$, is found abundantly in nature and forms the basis for the analcime group of zeolites that includes analcime, wairakite, leucite, and pollucite (see Table 1 for the formulas of all minerals referenced in the text). Analcime and analcime-group minerals have been shown to be efficient at removing ions of radionuclides elements from solutions (Sipos et al. 2010; Mallah et al. 2012; Shushkov et al. 2013; Jiménez-Reyes et al. 2021). The observed chemistry of natural and synthetic analcime can vary substantially from its idealized formula (Passaglia and Sheppard 2001; Neuhoff et al. 2003; Deer et al. 2004; International Zeolite Association 2023). The Ca-end-member of the analcime group, wairakite, $Ca(Al_2Si_4O_{12})\cdot 2H_2O$, has a crystal structure defined by a form of "true" monoclinic wairakite, as commonly identified in natural environments. A tetrahedral form of wairakite (or Ca-analcime) has additionally been observed as a product of laboratory synthesis (Seki 1968; Liou 1970; Neuhoff et al. 2003). A solid solution between the Na-end-member analcime and the Ca-end-member wairakite has been explored since wairakite was first identified (Coombs 1955; Steiner 1955; Seki and Oki 1969; Surdam 1973). Early studies characterizing wairakite and its mineralogical relationship to analcime described a compositional gap between $Anl_{45}Wrk_{55}$ and $Anl_{75}Wrk_{25}$ in natural samples, which was initially identified as an immiscibility region (Steiner 1955; Seki and Oki 1969). Later analyses (Passaglia and Sheppard 2001) have recognized an isomorphous series between the Na- and Ca-end-members such that analcime-group minerals with Na/(Na+Ca) > 0.5 can be classified as analcime and those with Na/(Na+Ca) < 0.5 as wairakite.

Analcime-group mineral formation has been observed as a product of hydrothermal alteration both of bentonites (de la Villa et al. 2001; Cheshire et al. 2014; Sauer et al. 2020) and of cements (Gaucher and Blanc 2006; Lothenbach et al. 2017). The presence of cement as a reactant, in particular, has been noted to promote analcime formation through increases in pH above that expected in solutions equilibrated with bentonite (Savage et al. 2007) or most repository host rocks (Kersting et al. 2012). Cement addition to these systems may additionally promote wairakite formation over analcime by increasing the availability of Ca in the system, particularly at higher temperatures that promote the stable formation of wairakite relative to clay minerals. As the cation exchange capacity of analcime is greater than that of wairakite (Ames 1966), characterizing the systems and reactants that drive mineral formation in the analcime-wairakite series is valuable for estimating the evolution of EBS properties over time.

To evaluate the abundance and type of zeolites that form during elevated-temperature interactions between clays and cement

Table 1. Chemical formulas for minerals referenced in the text

Mineral		Source	Formula
Analcime		IMA	$Na(AlSi_2O_6)\cdot H_2O$
Albite		IMA	$Na(AlSi_3O_8)$
Biotite		MinDat	$K(Mg,Fe)_3(OH,F)_2Si_3AlO_{10}$
Brownmillerite		IMA	$Ca_2Fe^{3+}AlO_5$
Calcite		IMA	$Ca(CO_3)$
Chlorite	(Chamosite)	IMA	$(Fe^{2+},Mg,Al,Fe^{3+})_6(Si,Al)_4O_{10}(OH,O)_8$
Clinoptilolite	(Clinoptilolite-Ca)	IMA	$Ca_3(Si_{30}Al_6)O_{72}\cdot 20H_2O$
Ettringite		IMA	$Ca_6Al_2(SO_4)_3(OH)_{12}\cdot 27H_2O$
Garronite	(Garronite-Ca)	IMA	$Ca_3(Al_6Si_{10}O_{32})\cdot 14H_2O$
Hatrurite		MinDat	Ca_3SiO_5
Heulandite	(Heulandite-Ca)	IMA	$(Ca,Na,K)_5(Si_{27}Al_9)O_{72}\cdot 26H_2O$
Illite		MinDat	$K_{0.65}Al_{2.0}[Al_{0.65}Si_{3.35}O_{10}](OH)_2$
Kaolinite		IMA	$Al_2Si_2O_5(OH)_4$
Larnite		IMA	$Ca_2(SiO_4)$
Leucite		IMA	$K(AlSi_2O_6)$
Montmorillonite		MinDat	$(Na,Ca)_{0.33}(Al,Mg)_2(Si_4O_{10})(OH)_2\cdot nH_2O$
Na-Montmorillonite		Analyzed	$(Na_{0.31},Ca_{0.04},K_{0.01})(Al_{1.53},Fe_{0.21},Mg_{0.18},Ti_{0.01})(Si_{3.98},Al_{0.02})O_{10}(OH)_2$
Opal		IMA	$SiO_2\cdot nH_2O$
Phrehnite		MinDat	$Ca_2Al_2Si_3O_{10}(OH)_2$
Plagioclase		MinDat	$(Na,Ca)[(Si,Al)AlSi_2]O_8$
Pollucite		IMA	$Cs(Si_2Al)O_6\cdot nH_2O$
Portlandite		MinDat	$Ca(OH)_2$
Pyrite		IMA	FeS_2
Quartz		IMA	SiO_2
Tobermorite		IMA	$Ca_4Si_6O_{17}(H_2O)_2\cdot(Ca\cdot 3H_2O)$
Wairakite		IMA	$Ca(Si_4Al_2)O_{12}\cdot 2H_2O$

Notes: Formulas included were sourced from the International Mineralogical Association (IMA 2008) and (MinDat 2024) databases. Minerals are titled as referenced in the text, and names in parentheses indicate the name of the mineral species for the formula listed in the source. Na-montmorillonite shows the formula of the WB used in the experiments, as previously analyzed and presented by Cheshire et al. (2014). "Smectite," "zeolite," and "Fe-oxide" as used in the text refer to groups of minerals.

materials, we conducted a set of experiments combining ordinary Portland cement powder with steel, Opalinus clay, and a synthesized Opalinus clay groundwater. The experiments were heated to 200 or 300 °C and reacted at temperature for 8–24 weeks. The results were used to evaluate the impact of uncured cement on the mineralogy of analcime-group zeolites expected to form under hydrothermal conditions in a spent fuel repository. Finally, our results are compared to previously published literature on the mineral chemistries of analcime and wairakite.

Methods

Hydrothermal experiments

Experiments were conducted using a Dickson-type, gold cell autoclave system as detailed by Seyfried et al. (1987). Briefly, this system consists of a flexible gold reaction cell (~120 mL) fixed within a 500 mL confined reactor and surrounded by an annulus of DI water. Pressure in the experiments was maintained at 15 MPa by pressurizing the water within the confining reactor. Temperature was controlled by a furnace surrounding the confining vessel, controlled by feedback from a thermocouple fitted within the confining vessel (Seyfried et al. 1987). The reaction cell was fitted with a titanium head that allowed fluid sampling during the experiments through an exit tube extending from within the reaction cell to the outside of the vessel.

Repository designs may include cement liners separated from steel waste canisters by bentonite buffers or specific inclusion of cement products near steel-cement interfaces (Bildstein et al. 2019; N s 2020; Fabian et al. 2023); the combined reactants in these experiments were selected to observe reactions of both bentonite and steels that may occur where the saturating groundwater chemistry is strongly affected by cement. Reactants, i.e., Opalinus clay as an analog repository wall rock, Wyoming bentonite (WB) to emulate bentonite buffer materials, ordinary Portland cement (OPC), powder, steel, and a synthetic Opalinus clay groundwater (GW) solution, were combined in the gold reaction cells and isothermally heated to 200 or 300 °C for the experimental durations of 8 or 24 weeks. Masses of reactants, experimental durations, temperatures, and additional experimental parameters are included in Table 2. Fluid samples were collected weekly throughout the experiment durations, with ~5–7 mL of solution removed from the reaction cell during each sampling event. As a result of sampling, the water-rock ratios decreased throughout the experimental duration, but remained within an order of magnitude, decreasing to between 7:1 and 5:1 at experiment termination. Solid samples remained saturated throughout the experiments, and the decreasing water-rock ratio was not expected to have impacted reaction processes beyond affecting the observed rates of fluid chemistry change. Fluid samples equilibrated to bench conditions (~25 °C, 1 atm) within minutes, and the pH of an unfiltered aliquot of the sampled fluid was measured directly (<2 min) after sampling. Aliquots of fluid samples collected before, during, and after the experiments that were used for anion and cation analyses (described below) were filtered using 0.22 µm syringe filters and stored in polytetrafluoroethylene vials at 1 °C. After experiment termination, the remaining solution was poured off into a cone filter, the remaining solid sample was removed from the reaction cell, and the steel billets were manually removed. When analyzed separately, Opalinus clay pieces were manually separated from the bentonite clay matrix. Solid samples were dried in a desiccator under air at 22 °C for 1–3 weeks. Selected pieces of each type of solid reactant (mixed clay-OPC, Opalinus clay, and steel billets) were then embedded in epoxy and prepared as thin sections or epoxy mounts for microscopy analyses. Steel billets were placed in epoxy, orthogonal to the polished surface, and cut through to allow observation of alterations at the steel-bentonite interfaces.

Materials

All experiments combined solid reactants with a synthetic GW solution that approximated the chemistry of Opalinus clay porewater as reported by Pearson et al. (2003) using Milli-Q ultrapure water (18.2 MΩ·cm) and analytical-grade salts. The target initial solution chemistry is reported in Table 3. Wyoming bentonite, Opalinus clay, and uncured OPC powder were included as solid reactants in all experiments. The WB was provided by Bentonite Performance Minerals LLC and sourced from a reducing horizon at Colony, Wyoming, U.S.A. The bentonite was pulverized and sieved to <3 mm before use. The initial mineral assemblage of the WB was predominantly Na-montmorillonite, with lesser amounts of clinoptilolite and feldspar, and minor biotite, pyrite, quartz, opal, and sulfide minerals. Opalinus clay was sourced from the Mont Terri Underground Rock Laboratory in Switzerland (drill core BFE-A10) and stored under air before use. The Opalinus clay used in the experiments was predominantly composed of clay minerals, with lesser amounts of carbonates and silicates. The OPC used in the experiments was type I/II uncured OPC powder purchased from Holcim US and selected for reactivity within the experimental time frame. Analysis showed the OPC to be largely composed of calcium silicates larnite, hatrurite, and brownmillerite; the complete analyzed mineralogy is included in Table 4. Redox conditions for each experimental system were buffered to the iron-magnetite field by adding a 1:1 mixture (by mass) of Fe_3O_4 and Fe^0; the combined metal buffers were added at ~0.07 wt% of the mass of the other solid and fluid reactants in each experiment. Billets of two types of stainless steel (316SS and 304SS) and a low-carbon steel (LCS) were also included as reactants in EBS-24 through EBS-28 (Table 2) to simulate co-alteration with waste canister materials.

Analytical methods

Analytical electron microscopy was performed using a FEI Inspect F scanning electron microscope (SEM) and a FEI Apreo SEM at Los Alamos National Laboratory. Secondary electron (SE) imaging with the SEM was performed using an accelerating voltage of 5.0 kV and a spot size of 10 nm. Backscatter electron (BSE) imaging and energy-dispersive X-ray spectroscopy (EDS) were performed at 30 kV and a 3.0 µm spot size. Electron microprobe (EMP) analyses were performed at the University of Oklahoma using a Cameca SX50 electron microprobe equipped with five wavelength-dispersive spectrometers and PGT PRISM 2000 energy-dispersive X-ray detector. BSE imaging coupled with energy-dispersive X-ray analysis was performed using beam conditions of 20 kV acceleration and

Table 3. Initial target chemistry for the synthetic Opalinus clay GW solution

Species	Concentration
Ca^{2+}	1.1E-02 mol L^{-1}
Cl^-	1.8E-01 mol L^{-1}
HCO_3^-	2.7E-03 mol L^{-1}
K^+	5.8E-03 mol L^{-1}
Na^+	1.7E-01 mol L^{-1}
Si	3.6E-05 mol L^{-1}
SO_4^{2-}	1.0E-02 mol L^{-1}
Sr^{2+}	1.8E-06 mol L^{-1}
pH	7.5

Table 2. Reaction parameters and initial reactant masses for EBS experiments

Exp.	(°C)	Duration	GW (g)	OC (g)	WB (g)	OPC (g)	Steel (type)	Steel (g)	Fe° (g)	Fe_3O_4 (g)	WRR
EBS-23	200	8 weeks	150	2.0	5.9	2.1	–	–	0.57	0.48	13.6
EBS-24	200	8 weeks	150	2.0	6.0	2.0	316	4.52	0.52	0.51	13.6
EBS-25	200	8 weeks	126	2.0	6.0	2.0	304	3.27	0.55	0.51	11.4
EBS-26	200	8 weeks	130	2.0	6.0	2.0	LCS	5.02	0.50	0.50	11.8
EBS-27	200	24 weeks	270	7.6	22.8	7.6	316	5.06	0.95	0.95	6.8
EBS-28	300	8 weeks	138	2.2	6.6	2.2	316	5.06	0.50	0.50	11.7

Notes: Exp. = experiment identifier; (°C) = reaction temperature; GW = groundwater solution; OC = Opalinus clay; WB = Wyoming bentonite; steel types are noted under Steel (type), where 316 = 316 stainless steel, 304 = 304 stainless steel; LCS = low-carbon steel; Fe° = iron filings; Fe_3O_4 = magnetite; and WRR = water:rock ratio (by mass), where measured by mass, all masses are reported as grams (g).

Table 4. Quantitative X-ray diffraction (QXRD) results of unreacted and reacted materials (wt%)

Phase	WB	OC	OPC	Mix	EBS-24	EBS-25	EBS-26	EBS-27a	EBS-27b	EBS-28
Non-clay fraction										
Quartz	1.5	14.0	–	5.2	4.9	1.9	3	tr.	1.9	3.9
K-feldspar	tr.	6.0	–	2.0	–	tr.	tr.	1.1	–	tr.
Plagioclase	6.2	3	–	3.1	5	1.3	1.6	1.4	1.3	11.8
Calcite	–	16.7	–	5.6	6.8	3	3.7	10.7	3.4	4.1
Dolomite	–	tr.	–	tr.	–	–	–	–	–	–
Gypsum	tr.	–	–	–	–	–	–	–	–	2.8
Halite	–	–	–	–	tr.	–	tr.	tr.	tr.	–
Pyrite	tr.	1.1	–	tr.	tr.	–	–	–	tr.	–
Clinoptilolite-heulandite	13	–	–	4.3	7.6	9.2	7.6	3.6	17.5	–
Cristobalite	1.5	–	–	tr.	–	–	–	–	–	–
Larnite	–	–	14.6	4.9	–	–	–	–	–	–
Hatrurite	–	–	67.1	22.4	–	–	–	–	–	–
Brownmillerite	–	–	16	5.3	–	–	–	–	–	–
Analcime-wairakite	–	–	–	–	1.3	4.4	4.2	30.9	14.4	6.8
Garronite	–	–	–	–	8.5	10.8	9.9	5.6	10.0	2.5
Magnetite	–	–	–	–	2.4	–	–	tr.	–	2.9
Tobermorite	–	–	–	–	1.8	1.4	2.7	8.7	3.2	4.5
Amorphous	–	–	2.3	tr.	7.8	6.6	3.8	7	2	1.6
Total	22.2	40.8	100	52.7	46.1	38.6	36.5	69.0	53.7	40.9
Clay fraction										
Smectite+illite+I/S	71	24.5	–	31.8	40.1	54.5	51.3	23.8	42.3	55.3
Mica	3.8	7.5	–	3.8	6.4	5.3	6.1	3.7	2	3.4
Chlorite	2	9.2	–	3.7	tr.	–	–	–	–	–
Kaolinite	–	17.2	–	5.7	6.9	1.6	4.7	1.3	1.2	–
Total	76.8	58.4	0	45.1	53.4	61.4	62.1	28.8	45.5	58.7

Notes: WB = Wyoming bentonite; OC = Opalinus clay; OPC = ordinary Portland cement; Mix = calculated mineralogical abundances at the ratio of reactants used in experiments (60:20:20 WB:Opalinus clay:OPC). "–" indicates below the mineral was not detected at the instrument detection limits (~0.5 wt%); "tr." indicates that peaks were identified but the mineral abundance was estimated to be below 1 wt%: columns may not sum to 100% because of this convention. The average mineral abundance error for each phase is approximately ±1 wt% for the non-clay fraction and ±5 wt% for the clay.

20 nA sample current. Quantitative chemical analyses were performed by wavelength-dispersive spectrometry with an accelerating voltage of 20 kV, beam current of 20 nA, and spot size of 2 μm. Matrix corrections employed the PAP algorithm (Pouchou and Pichoir 1985), with oxygen content calculated by stoichiometry. Counting times were 30 s on peak for all elements. Minimum levels of detection (calculated at 3σ above mean background) in the range of 0.01 to 0.03 wt% of the oxides for all components except F (0.16 wt%). All standards for elements in the silicates were analyzed using 30 s count times on peak and *K*α emissions. Results from EMP analyses are included in Online Materials[1] Table S1.

Solid samples were ground with 20 wt% corundum before quantitative X-ray diffraction (QXRD) analyses (Chung 1974). QXRD measurements for EBS-24 and -25 were completed with a Siemens D500 diffractometer using Cu*K*α radiation. Data were collected from 2 to 70 °2θ with a 0.02 °2θ step size and count times of 8 to 12 s per step. Quantitative phase analysis was performed using FULLPAT (Chipera and Bish 2002) and Jade 9.5 X-ray data evaluation software, with the ICDD PDF-4 database (Kabekkodu et al. 2002). XRD analyses for EBS-26, -27, and -28 were conducted on a Bruker D8 Discover using Cu*K*α radiation (λ = 0.154 nm, 40 kV, and 40 mA) and a silicon drift detector. Quantitative phase analyses were performed using whole-pattern fitting with Jade 9.5 X-ray data evaluation software, utilizing the ICDD PDF-4 database. The mineral abundance error for each phase for all analyses is approximately ±3.5 wt% for non-clay minerals and ±6 wt% for clay minerals. Illite, smectite, and mixed-layer illite-smectite, along with clinoptilolite-heulandite and analcime-wairakite, are reported together as a combined fraction due to analytical challenges in distinguishing between these phases using the employed methods.

Clay XRD analyses were performed using a Bruker D8 Discover with Cu*K*α radiation. To isolate the clay fraction, <2 μm particles were separated via sedimentation in deionized H_2O. An aliquot of the <2 μm suspension was dropped on a zero-background quartz plate and dried. This oriented mount was analyzed from 2 to 40 °2θ at 8 to 12 s per step. The oriented mount was then saturated with ethylene glycol in a 60 °C oven for 24 h, and XRD analysis was repeated. A portion of the >2 μm particles was ground with a mortar and pestle, deposited on a zero-background quartz plate, and X-rayed under the same parameters as the bulk powder material. The remaining portion (>2 μm) was used for electron microscopy. Mineral identification and unit-cell parameters analysis were performed using Jade 9.5 X-ray data evaluation program with ICDD PDF-4 database. Expandable component abundances for the disordered illite-smectites were calculated via the D°2Q method (rodo 1980; Moore and Reynolds 1989; Eberl et al. 1993). A regression from calculated data was used to calculate the percent expandable (%Exp) component in each untreated and reacted bentonite by the following equation:

$$\%\text{Exp} = 973.76 - 323.45\Delta + 38.43\Delta 2 - 1.62\Delta 3$$

[Eberl et al. (1993) Eq. 3, $R^2 = 0.99$ (1)

with Δ corresponding to D°2Q between the 002 and 003 peak positions for the oriented ethylene-glycol-saturated samples. Results are shown in Online Materials[1] Figure S1 and Table S2.

Bulk geochemistry of the initial reactants and post-mortem solid reactants was analyzed by X-ray fluorescence (XRF) using a Rigaku Primus II wavelength-dispersive XRF spectrometer. Samples were first crushed and homogenized in 5–10 g portions in a tungsten-carbide ball mill. Sample splits were heated at 110 °C for 4 h, then allowed to equilibrate at ambient laboratory conditions for 12 h to minimize weighing errors from atmospheric water gain. Fusion disks were prepared for analyses of the samples by mixing 1.25 g aliquots of sample with 8.75 g of lithium metaborate-tetraborate flux and heating the mixture in a muffle furnace for 45 min at 1050 °C. All reported values exceed three times the reported detection limits. Additional 1 g aliquots from each sample population were heated at 1000 °C to obtain the loss-on-ignition measurements used in the data reduction program. Results are included in Online Materials[1] Table S3.

Major cations and trace metals in the solution were analyzed via inductively coupled plasma optical emission spectrometry (ICP-OES, Perkin Elmer Optima 2100 DV) and inductively coupled plasma mass spectrometry (ICP-MS, Elan 6100) using EPA methods 200.7 and 200.8. Ultrahigh-purity nitric acid was used in the preparation of samples and calibration standards prior to analysis. Internal standards (Sc, Ge, Bi, and In) were added to samples and standards to correct for matrix effects. The Standard Reference Material 1643e Trace Elements in Water method was used to verify the accuracy of the multi-element calibrations. Inorganic anion samples were analyzed by ion chromatography (IC) following EPA method 300 on a Dionex DX-600 system. Selected aqueous chemistry results are shown in Online Materials[1] Figure S3, and complete results are included in Online Materials[1] Tables S4–S9.

Geochemical modeling

In situ pH, speciation, and dissolved species activities at experimental temperatures were calculated using PHREEQC v.3.7.3 with the ThermoddemV1.10_15Dec2020.dat database (Blanc et al. 2007), which uses the B-dot ion association

model. This database was selected for its application to modeling waste repository geochemistry and its temperature range (to 300 °C). Calculations assumed HCO_3^- concentrations consistent with the mass initially included in the GW solutions (2.7×10^{-3} mol L^{-1}, Table 3). Equilibrium aqueous speciation and in situ pH for each sample were then calculated by first computing aqueous speciation for the analyzed solution chemistry of each sample at 25 °C, followed by recalculation of pH and solution speciation at experimental conditions. Additional information on model parameters, including background solution chemistry and mineral chemistry used in stability field calculations, is included in Online Materials[1] Table S10.

Results

Crystal chemistry (SEM and EMP)

Zeolite phases were found throughout the reaction products from the 8-week experiments run at 200 °C (EBS-23 through EBS-26). Analcime-type zeolite minerals were associated with each of the solid reactants: (1) in the fine-grained clay (bentonite) groundmass; (2) at the Opalinus clay-bentonite interface; (3) in the porous OPC matrix; and (4) at the steel-clay/OPC interface (Fig. 1). Analcime-group minerals with Na/(Na+Ca) > 0.5 are referred to as analcime and those with Na/(Na+Ca) < 0.5 as wairakite. After reaction, masses of OPC identified as distinct from the clay matrix were largely observed as porous matrices of calcium-silicate-hydrate (CSH) and calcium-(alumino)-silicate-hydrate [C(A)SH] phases, with analcime crystals throughout (Fig. 1a). On the recovered chips of Opalinus clay, analcime crystals were consistently found to have formed in abundance at the Opalinus clay-bentonite interface (Fig. 1b). At the steel surfaces, analcime was identified at the surface forming isolated rounded crystals of ~10 μm (Fig. 1c). Analcime was also observed in mat-like structures formed at reacted steel surfaces and were similar in form on all types of steel reacted in the experiments (316SS, 304SS, and LCS).

Analcime-group minerals identified in the long-term (24-week) experiment reacted at 200 °C (EBS-27) had several notable differences from those detected in the short-term (8-week) 200 °C experiments (EBS-23 through -26). Specifically, the maximum size of individual crystals or rounded crystal agglomerations was larger, reaching ~50 μm diameter (Figs. 1d and 1e). This was true in the clay matrix and in OPC, as well as at the steel surface. The chemistry of the crystals at the reacted steel surface was identified as Ca-rich [Na/(Na+Ca) < 0.5] by EDS and EMP analyses (Fig. 1f). CSH minerals were also identified in greater abundance throughout the clay matrix in EBS-27 compared to EBS-23 through -26.

In the materials reacted in EBS-28 at 300 °C, the analcime-group minerals identified in all matrices in EBS-28 were relatively Ca-rich (compared to those identified in the 200 °C

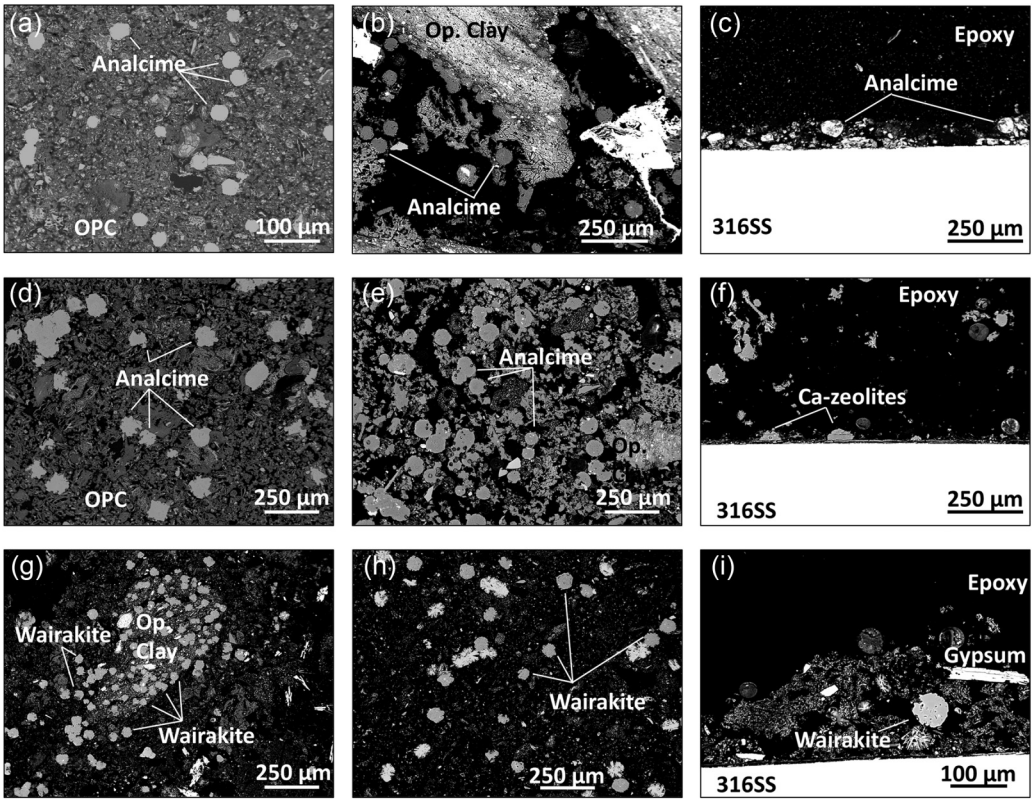

Figure 1. BSE images of reactants from EBS-24, -27, and -28, including analcime-wairakite minerals. Panels (**a**, **b**, **c**) show reactants from EBS-24 (200 °C, 8 weeks): (**a**) remaining OPC matrix with secondary analcime; (**b**) analcime formed in the reacted clay matrix; (**c**) analcime formed at the surface of reacted 316SS. Panels (**d**, **e**, **f**) show reactants from EBS-27 (200 °C, 24 weeks): (**d**) secondary analcime in a CSH matrix of reacted OPC; (**e**) analcime formed in the reacted clay matrix; (**f**) Ca-bearing zeolite minerals at the reacted 316SS surface. Panels (**g**, **h**, **i**) show reactants from EBS-28 (300 °C, 8 weeks): (**g**) an abundance of wairakite formed within an Opalinus clay fragment; (**h**) wairakite formed in the reacted clay matrix; (**i**) wairakite formed at the reacted 316SS surface.

experiments) and were identified as wairakite by EMP analysis. Wairakite was within and around identified Opalinus clay chips (Fig. 1g), as well as within the reacted clay matrix (Fig. 1h). In the clay matrix, wairakite crystals were dominantly 10–20 μm diameter, similar to the size of analcime crystals identified in EBS-23 through -26 at 200 °C (Figs. 1g and 1h). Wairakite crystals identified at the reacted 316SS surface exceeded 50 μm (Fig. 1i). As in EBS-27, CSH phases were observed throughout the clay matrix. No OPC grains nor anhydrous cement phases were identified as discrete from the clay matrix.

EMP analyses of the chemistry of the analcime-group zeolite grains identified in the experiments showed differences in zeolite chemistry within each experiment based on the initial reactants with which they were associated. The composition of the analcime formed in EBS-23 to -26 (reacted for 8 weeks at 200 °C) spanned a range of Na/(Na+Ca) compositions from >~0.5 to <0.8, consistent with analcime having substantial Ca incorporated in place of Na. The Si/Al values for these zeolites were dominantly between 2.0 and 2.5. Compositional differences in the analyzed analcimes were not associated with different contexts (i.e., clay matrix, encrusting Opalinus clay fragments, OPC, steel) in EBS-23 through -26. In the 24-week experiment (EBS-27), analcime-type zeolite minerals identified in the clay matrix and remaining OPC fractions generally covered the same range of Na/(Na+Ca) and Si/Al as those observed in the 8-week experiments (Fig. 2). The zeolite minerals formed at the steel surfaces were compositionally wairakite and substantially Ca-rich compared to those formed in the 8-week experiments, with Na/(Na+Ca) < 0.22. However, many analyzed points of the zeolite minerals at the steel surface from EBS-27 also had Si/Al ratios substantially exceeding the maximum accepted Si/Al ratio for wairakite of ~3 (Passaglia and Sheppard 2001). These analyses were excluded from further data interpretation, including the calculation of averaged values. In EBS-28, reacted for 8 weeks at 300 °C, zeolite phases analyzed in all contexts within the reaction products were compositionally wairakite [Na/(Na+Ca) < 0.28, Fig. 2]. The Si/Al ratios of the wairakite identified in the EBS-28 reaction products were broadly distributed between 1.9 and 3.2. We note that the results of many of the analcime-wairakite EMP analyses show a small negative charge balance (<5%), suggesting potential sodium migration from subhedral zeolite phases during excitation or during thin section preparation. EMP analyses with charge balance >10% were excluded from the data set.

Bulk mineralogy and geochemistry (XRD and XRF)

QXRD results showed that newly formed and increased mineral phases after reaction included analcime-wairakite, garronite, tobermorite, and amorphous material (Table 4). None of the initial OPC minerals, larnite, hatrurite, brownmillerite, or portlandite, a major component of cured OPC, were identified after the experiments. QXRD analysis was not performed on the sample from EBS-23 due to the small amount of solid sample

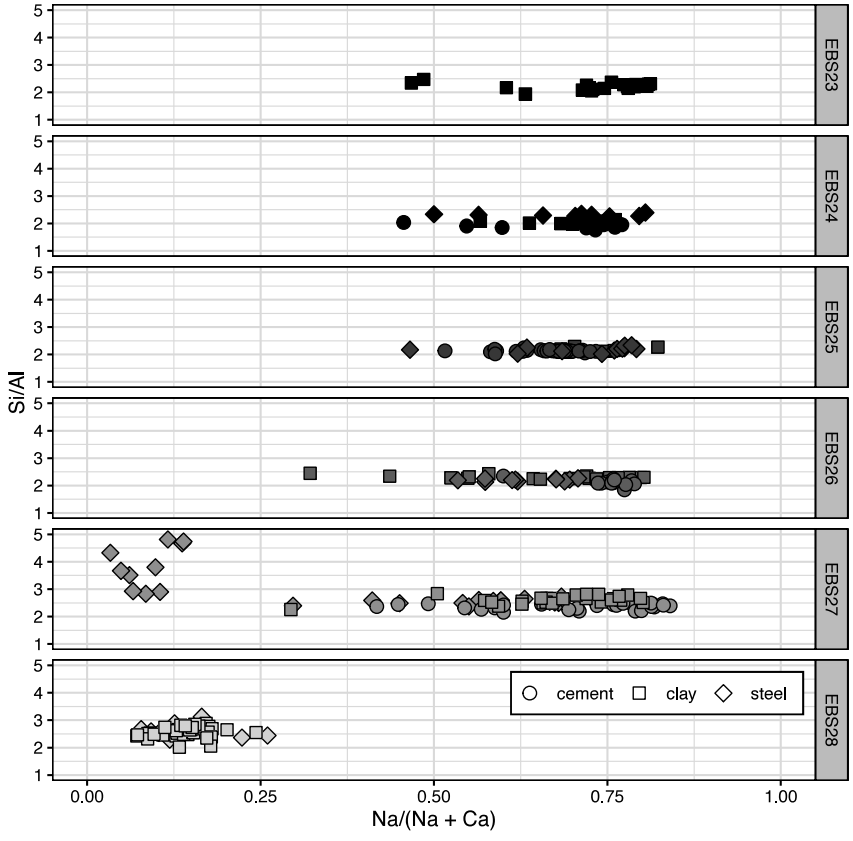

Figure 2. Chemical compositions of zeolites grouped by experiment. Markers indicate the location of the analyzed zeolite within the reactant mix. The *x*-axis indicates the relative proportion of Na to the total compositional Na+Ca, where 0.00 indicates a composition consistent with end-member wairakite and 1.00 indicates a composition consistent with analcime. The *y*-axis shows the Si/Al ratio of the analyzed points.

recovered. After the experiments at 200 °C, the mass% of the clinoptilolite-heulandite group zeolite was preserved in the 8-week experiment and increased in the 24-week experiment (EBS-27). The solid reaction products of EBS-27 were observed to be physically stratified in the reaction cell after experiment termination, potentially due to the greater initial mass of solid reactants, lower initial water-rock ratio, and/or longer experimental duration (24 weeks as opposed to 8 weeks). Solid reactants collected from EBS-27 were then divided and analyzed based on their depth in the reaction cell: sample EBS-27a was collected from the top of the solid reaction products, while EBS-27b was collected from the solids that had been located at the bottom of the gold bag during reaction. The orientation "top" and "bottom" of the reaction cell refer to their positions during the reaction, when the water-saturated solid reactants settle to the bottom of the bag. EBS-27a had a higher abundance of analcime-wairakite and calcite and a substantially lower abundance of clay phases compared to EBS-27b. In the solid reaction products from the 300 °C experiment (EBS-28), we observed the formation of abundant wairakite and CSH phases and relative increases in plagioclase feldspar. In contrast to the experiments at 200 °C, no peaks from clinoptilolite-heulandite were observed in the reacted products. Clay XRD analyses of oriented clay fractions from the clay groundmass showed reduced expandability of the clay phase after reaction (Online Materials[1] Fig. S1 and Table S2). Shifts of the glycolated smectite (GS) 002 and 003 peaks from the 2 μm fraction of the clay groundmass correspond to ~10% reduction in expandability in the 8-week, 200 °C experiments, as well as in the 8-week, 300 °C experiment (EBS-28). The expandability of the clay phase after EBS-27 (24 weeks, 200 °C) was not quantified; the amorphous phases in the sample were presented as a broad peak between 18 and 25 °2θ, which obscured the position of the d003 glycolated smectite peak.

XRF analyses showed that the solid samples generally decreased in Ca and Si and increased in Na after reaction (Online Materials[1] Table S1). Solid reactants from the 24-week experiment (EBS-27) were divided and analyzed based on their depth in the reaction cell in the same manner as for XRD analysis described above. EBS-27a was taken from the top layer inside the reaction cell and contained higher concentrations of CaO and Fe_2O_3 in comparison to EBS-27b (16.4 vs. 11.6 wt% and 8.4 vs. 7.5 wt%, respectively), which was taken from near the bottom of the reaction cell. EBS-27b had a higher wt% of SiO_2 and Al_2O_3 compared to EBS-27a (49.5 vs. 41.5 wt% and 15.4 vs. 13.7 wt%, respectively), consistent with the greater mass% of clay minerals in EBS-27b (Table 4). In the 300 °C experiment (EBS-28), Fe_2O_3 was elevated in the reaction products in comparison to the unreacted starting material.

Aqueous chemistry

In all experiments conducted at 200 °C, the pH was observed to fluctuate by several pH units during the first 2–3 weeks of experimental time before achieving an apparent steady-state bench pH of 8.5–9. Samples from EBS-28 (300 °C) stabilized at a substantially lower pH of ~6 after an initial upward fluctuation to pH >9 in the first week (as measured at ambient conditions). K and Na concentrations in the 200 °C experiments (EBS-23 through -27) had divergent trends, with EBS-23 and -24 having lower K and Na concentrations compared to EBS-25 through -27. Samples from EBS-23 and EBS-24 had initial trends of $K < 0.003$ mol L^{-1} and $Na < 0.1$ mol L^{-1}. In contrast, experiments EBS-25 through -27 had consistently higher K and Na concentrations ($K > 0.004$ mol L^{-1} and $Na > 0.13$ mol L^{-1}). At 300 °C (EBS-28), K concentrations increased and then remained elevated (>0.005 mol L^{-1}) for the remainder of the experiment. Na concentrations were initially elevated, then sharply decreased after the second week of reaction. Ca concentrations remained constant (EBS-23 and -24) or gradually increased (EBS-25 through -27). While steady-state concentrations of Na and K were apparently achieved after ~10 weeks in the long-term experiment EBS-27, Ca concentrations continued to increase throughout the 24-week duration of EBS-27. EBS-28 conducted at 300 °C had similar Ca concentrations in magnitude to those from 200 °C. In the 200 °C experiments (EBS-23 through -27), SiO_2 increased to final concentrations of $\sim 5 \times 10^{-3}$ to 7×10^{-3} mol L^{-1}. In EBS-28 (300 °C), the final SiO_2 concentration was substantially higher ($\sim 1.7 \times 10^{-2}$ mol L^{-1}). Al and Mg were below detection limits for most of the experimental durations. Complete aqueous chemistry results are illustrated in Online Materials[1] Figure S2 and included in Online Materials[1] Tables S1–S6.

Discussion

Cement-clay interactions and zeolite formation

In general, the formation of analcime-group zeolites in hydrothermal conditions is promoted by increased Na^+, Ca^+, and pH, as well as by dissolved SiO_2 concentrations equilibrated with quartz (Kerrisk 1983; Chipera and Apps 2001). For example, hydrothermal clay alteration is known to produce zeolites by the following generalized reactions (Bayliss and Levinson 1971; Mosser-Ruck et al. 2016):

$$3\,\text{smectite} + 3\,\text{Fe} + 4\,H_2O \rightarrow \text{chlorite} + 3\,\text{quartz} + 2\,\text{albite} + 3\,H_2 + \text{zeolite} \quad (2)$$

$$\text{calcite} + \text{quartz} + \text{kaolinite} + H_2O \rightarrow \text{garronite} + CO_{2(gas)} \quad (3)$$

Clinoptilolite, an accessory mineral in the bentonite phase, may also alter to analcime in hydrothermal conditions by the following generalized reaction:

$$\text{clinoptilolite} + 6\,Na^+ \rightarrow \text{analcime} + 24\,SiO_2 + 14\,H_2O + 3\,Ca^{2+} \quad (4)$$

After the 8-week experiments, at 200 °C, changes in the mineral phases derived from the WB and Opalinus clay were largely within the range of measurement error and natural sample heterogeneity. In the short term (after the 8-week experiments), the formation of analcime-wairakite and garronite zeolite minerals is interpreted to have been driven by the alteration of cement minerals. However, after 24 weeks of reaction (EBS-27), a relative decrease in smectite-illite minerals and an increase in clinoptilolite-heulandite were observed. As the mass percent of calcite was also generally preserved, this suggests a shift over

time to zeolite formation driven by alteration of the bentonite minerals, as per Equation 2, rather than Equation 4. At 300 °C (EBS-28), the lack of identification of any clinoptilolite-heulandite group minerals suggests that the formation of analcime-group minerals may have proceeded by Equation 4 or a similar reaction path that resulted in the formation of the more Ca-rich end-member, wairakite, with less Ca^{2+} release.

Analcime-wairakite formation in our experiments was abundant in comparison to previous hydrothermal studies that reacted WB without cement and resulted in minor or no formation of analcime-wairakite minerals (Cheshire et al. 2013; Caporuscio et al. 2017; Sauer et al. 2020; Zandanel et al. 2022). For example, Sauer et al. (2020) reported the formation of analcime as a minor phase (0.3–2.9 wt%) after 6–24 weeks of reaction of WB with Opalinus clay and Opalinus clay GW at 300 °C, and no analcime was identified in their experiments performed at 200 °C (as compared to 4.9–6.4 wt% analcime in EBS-23 through -26 reacted at 200 °C). Cheshire et al. (2014) similarly reported 1–3 wt% of high-Si analcime formed after WB was reacted in a brine solution at 300 °C for 5 weeks. The abundant formation of analcime-wairakite in our experiments is then attributed in part to the cement influence on fluid chemistry, as the inclusion of OPC in our experiments resulted in increased pH compared to these previous experiments, which is known to increase analcime stability and drive analcime-group zeolite precipitation (Chermak 1992; Savage et al. 2007).

Montmorillonite alteration to illite in hydrothermal conditions may result in a source of SiO_2 and Na in solution (Eberl and Hower 1976; Whitney 1990). Increases of SiO_2 in solution have been shown to be reliable indicators of illitilization (Cuadros and Linares 1996); however, as our experiments included mixed-mineral assemblages (rather than purified bentonite), the source of the observed increases in aqueous SiO_2 concentrations in our experiments was not unambiguously determined. Clay XRD analyses of the reacted clay matrices showed a 5–15% reduction in expandability and a ~10 to 20% increase in illite after most experiments, consistent with the observed decreases in dissolved K concentrations and increases in aqueous SiO_2 throughout the experiment. The resulting release of Na would also promote analcime formation and stability.

Analcime-wairakite formation

Analcime and analcime-wairakite were most abundant after the experiment with the longest reaction time (24 weeks, EBS-27), and greater abundances of analcime and wairakite were found in EBS-27a compared to EBS-27b (Table 4). The increased analcime-wairakite formation in EBS-27a may be attributed to increased interaction between the solid reactants and the Opalinus clay GW solution. Increased water-rock interaction is expected to have occurred in the solid that composed EBS-27a, at the top of the reaction cell, along with increased rates of water-mediated hydrothermal alteration. Bentonite swelling appeared to have excluded water from the bottom of the reaction cell, resulting in effectively lower water-rock ratios and limited fluid transport in the solid reactants at the bottom of the cell. For this reason, results from EBS-27a are considered comparable to those from EBS-24 through -26 that had higher water-rock ratios and smaller masses of initial reactants, while the reaction products in EBS-27b represent potential reaction pathways in a less water-saturated regime. Linear regression through the total of analcime+wairakite mass% in the solid phase after 0, 8, and 24 weeks show that analcime increased by ~0.6 to 1 wt% per week (Online Materials[1] Fig. S3). These values are obviously gross estimates and do not capture any changes in the formation rate over time, as would be expected during mineral precipitation in natural systems. In addition, the formation of analcime during the first 8 weeks of reaction is interpreted to be dominantly driven by the alteration of cement minerals, rather than bentonite. However, the decrease in clay minerals and increase in zeolite minerals in EBS-27 (in particular EBS-27a) indicate the potential for substantial bentonite alteration at cement interfaces under water-saturated conditions, or where fluid transport may provide a continuous input of groundwater over time.

The Na proportion, or Na/(Na+Ca), observed in the zeolites was affected by: (1) the reaction duration and (2) the reaction temperature. In experimental runs of up to 8 weeks at 200 °C (EBS-23 through -26), nearly all of the analcime-group minerals analyzed by EMP were found to be compositionally analcime, Na/(Na+Ca) > 0.5, with Ca as a subordinate cation. The Si/Al ratios for the analcime identified in EBS-23 through -26 were generally higher than the ideal formula for analcime (Si/Al = 2), consistent with elevated Si/Al ratios found in sedimentary analcimes (Passaglia and Sheppard 2001). The 24-week reaction time in EBS-27 resulted in the increased formation of both analcime and wairakite: EBS-27a and -27b had substantially greater proportions of analcime in the reacted mineral assemblage than in the 8-week experiments EBS-24 through -26 (Table 4). Hydrothermal alteration of the reactants at 300 °C and 8 weeks (EBS-28) resulted in greater wairakite formation and lesser analcime formation compared to the experiments run at 200 °C for 8 weeks (Table 4); all analyzed analcime-group minerals in EBS-28 were found to be wairakite compositions (Fig. 2) with the Si/Al variability within the ranges tabulated for natural wairakite (Passaglia and Sheppard 2001).

Overall, the result that wairakite was most abundant in the reaction products from EBS-28, reacted at 300 °C, is consistent with thermodynamic analysis showing increased wairakite stability at 300 °C compared to 200 °C (Online Materials[1] Fig. S4). The stability of wairakite relative to other minerals, specifically smectite minerals, is highly dependent on Si activity in hydrothermal conditions. At both 200 and 300 °C, increased silica activity in solution results in an increased smectite stability relative to analcime and wairakite. The long-term stability of analcime-group zeolites is then expected to be dependent on continued sources of dissolved Na and Ca in solution, such as through cation exchange with clay minerals or dissolution of cement phases, as observed here. Finally, increased pH also substantially increased the stability of analcime-wairakite zeolites. The elevated pH in our experiments driven by OPC is then interpreted to have been a major driver in the observation of analcime at 200 °C in these experiments, as compared to previous experiments reacting WB at 200 °C that had lower in situ pH and did not identify any analcime-group minerals (Sauer et al. 2020).

Reactions at steel surfaces

Mineral assemblages identified at the reacted steel surfaces in EBS-23 through -28 included zeolites (analcime, wairakite,

garronite, and ettringite), smectite minerals, C(A)SH phases, and Fe-oxides (Fig. 3), as well as some silicate crystals chemically consistent with a prehnite composition (as measured by EDS). The results contrast with previous work, where steel billets were reacted with WB under hydrothermal conditions, which produced the widespread formation of Fe-smectite or saponite at the steel-bentonite interface (Cheshire et al. 2018; Sauer et al. 2020). The difference can be attributed to the addition of OPC, as decreased steel corrosion is expected in aqueous solutions with elevated pH (Kursten et al. 2004). Additionally, even low concentrations of dissolved iron in solution have been shown to promote analcime formation under hydrothermal conditions (Katsuki et al. 2007) and may be incorporated into the analcime structure at up to several weight percent (Katsuki et al. 2007; Azizi and Yousefpour 2011). Many of the chemical analyses of analcime-wairakite minerals identified in our experiments contained trace iron that was particularly high among some samples from steel surfaces (up to 2 wt% FeO, Online Materials[1] Table S1). We posit that the alkaline pH of the bulk system and the differences in bulk chemistry in our experiments with uncured OPC powder inhibited steel corrosion, and the iron released promoted the formation of analcime-group minerals that were observed to coat the surfaces of all steel types, regardless of temperature.

In EBS-27, a population of zeolites observed at the reacted 316SS surfaces was found to have a substantially higher Ca component, Na/(Na+Ca) < 0.22, compared to both the analcime-group minerals identified in the reacted clay matrix in EBS-27 and those formed on the steel in all other experiments. The steel-surface zeolite population in EBS-27 also had exceptionally high Si/Al values, Si/Al > 3, and greater Si/Al variability compared to all other analyzed populations (Fig. 2). Samples prepared in cross section of the 316SS reacted in EBS-27 demonstrated petrographic evidence of intergrown analcime and garronite in the mottled textures of a zeolite at the steel-bentonite interface (Fig. 3b). These points are attributed to potential intermixing of analcime with garronite, prehnite, and/or C(A)SH phases that were observed to form in EBS-27; the EMP analyses from apparent mixed-phase points were excluded from aggregated data analyses. The visual evidence of the intergrowth and its range of compositions additionally suggests that the experimental conditions captured an overlapping or shifting of the garronite-analcime thermodynamic stability space.

Analcime-wairakite solid solution

For naturally formed analcime-group minerals, increases in Na/(Na+Ca) correspond to increased Si/Al variability (Passaglia and Sheppard 2001). This variability is particularly associated with tetrahedral analcime and tetrahedral Ca-analcime, whereas monoclinic wairakite has been reported to have less Si/Al disorder and less variability in Si/Al ratios (Neuhoff et al. 2003). A series of previous experiments that hydrothermally reacted water-saturated bentonite clay with various other components up to 300 °C resulted in hydrothermally formed zeolite minerals with compositions along the analcime-wairakite solid-solution (ss) series (Cheshire et al. 2013; Sauer et al. 2020). Reaction of WB in NaCl brines at 300 °C resulted in the formation of Si-rich analcimes (Fig. 4). Further experiments (Sauer et al. 2020) that reacted WB with Opalinus clay and a synthesized Opalinus clay GW at 200–300 °C also observed a range of Si-rich zeolites along the analcime-wairakite ss series. We note that measurements of Si/Al in analcime reported by Cheshire et al. (2014), as well as those reported by Bargar and Beeson (1981) and Vitali et al. (1995), exceeded the accepted Si/Al range (~1.50–2.92) for the analcime-wairakite group as described in Passaglia and Sheppard (2001).

Linear regression through the data that delineate the upper bound of Si/Al in Figure 4 (Vitali et al. 1995; Steiner 1955; Pe-Piper and Miller 2002; Sauer et al. 2020; Cheshire et al. 2013) describes the following empirical relationship between increases in Si/Al variability and Na/(Na+Ca):

$$\mathrm{Si/Al} = 1.53[\mathrm{Na}/(\mathrm{Na} + \mathrm{Ca})] + 1.90 \quad (5)$$

Previous studies have posited that Si/Al replacement in analcime is a function of temperature, pressure, and silica activity in solution (Neuhoff and Ruhl 2006) and that Si/Al replacement in wairakite, or deviation from long-range Si/Al order, occurs in tetragonal Ca-analcime and is not favored in monoclinic "true" wairakite (Neuhoff et al. 2003). Our results of the increasing Si/Al ratio with increasing Na/(Na+Ca) are then consistent with the formation of a series from monoclinic wairakite to analcime. The formation of Ca-rich end-members (wairakite) may additionally be promoted by increased Al ordering in the mineral structure (Aoki and Minato 1980). However, many of the previous studies reported Si/Al relationships for analcime and wairakite samples closer to the end-member compositions of those minerals than within the range of analyzed data presented here,

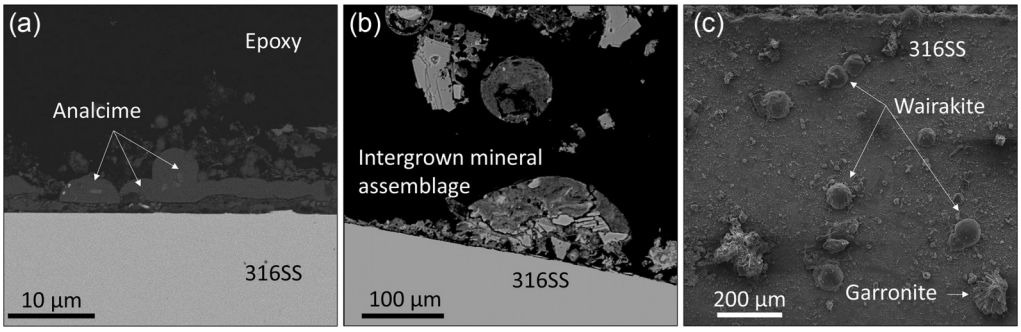

Figure 3. BSE images of analcimes formed at the steel surface and in the clay matrix. (**a**) Cross section of steel reacted in from EBS-26 mounted in epoxy, with analcime crystals and mat visible. (**b**) 316SS reacted in EBS-27 with intergrown secondary mineral assemblage at the surface. (**c**) 316SS surface from EBS-27 with wairakite and garronite.

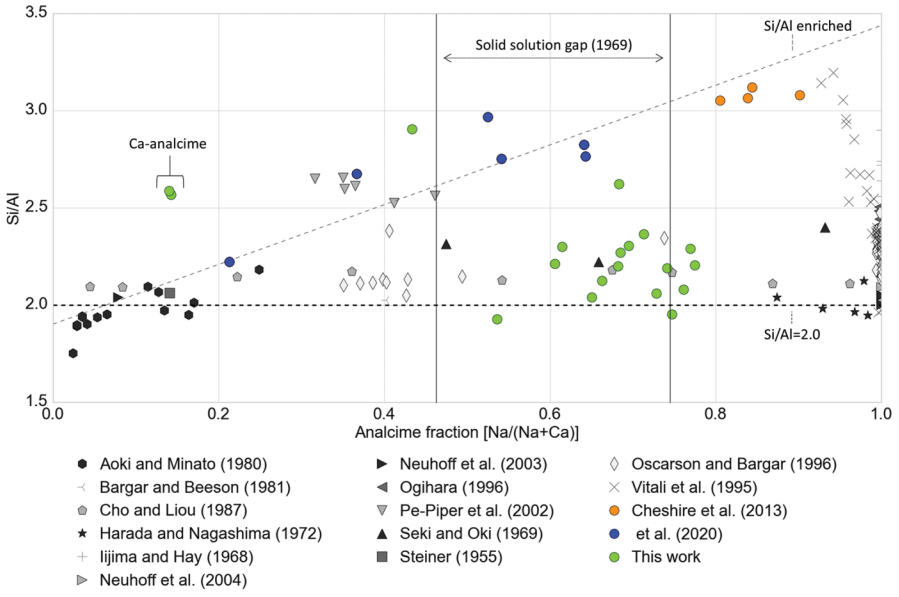

Figure 4. Analyses from this work and previous literature in analcime-wairakite solid-solution space. Two apparent trends are delineated: (1) the ideal Si/Al ratio (2.0) and (2) a trend of silica-enriched zeolites (Eq. 5). Analyses from this work and from experimental work published by Sauer et al. (2020) and Cheshire et al. (2013) fall along this line and fill in the gap from $Anl_{45}Wrk_{55}$–$Anl_{75}Wrk_{25}$. Additional data plotted from Steiner (1955), Iijima and Hay (1968), Seki and Oki (1969), Harada and Nagashima (1972), Aoki and Minato (1980), Bargar and Beeson (1981), Cho and Liou (1987), Vitali et al. (1995), Ogihara (1996), Oscarson and Bargar (1996), Pe-Piper and Miller (2002), Neuhoff et al. (2003, 2004), Cheshire et al. (2013), and Sauer et al. (2020). (Color online.)

with 0.30 > Na/(Na+Ca) < 0.70. Analysis of the data presented here suggests that increases in Si/Al and Ca/Na ratios follow a predictable relationship during analcime-wairakite formation, which can be further correlated with reaction temperature, depth of burial, and solution chemistry parameters known to affect Si/Al, Si-Al ordering, and analcime-wairakite composition.

Implications

The most reliable predictors of the relative dominance of analcime or wairakite in our experiments were: (1) the duration of the experiment and (2) the reaction temperature. At 200 °C, a longer experimental duration (24 weeks) resulted in analcime, Na/(Na+Ca) > 0.5, that had slightly increased Na content, Na/(Na+Ca), compared to experiments with shorter (8 weeks) durations. The increased reaction time also resulted in an increased formation of both analcime and wairakite, where analcime, as a mass percent of the final solid reactant assemblage, increased with experimental duration in an apparently linear relationship. Selected wairakite groups formed at 300 °C that had Si/Al ratios elevated over the ideal 2:1. As the kinetic transition from comparatively Si-rich Ca-analcime phases to monoclinic wairakite is sluggish, it is possible that longer reaction times at 300 °C would result in wairakite with decreased Si/Al ratios, similar to laumontite-wairakite transitions at elevated temperatures (Jove and Hacker 1997). In a subsurface backfilled nuclear waste repository, this would suggest that during heating where bentonite and OPC interact in the presence of fluids, analcime would form at temperatures <300 °C while at 300 °C the formation of Ca-analcime would be initiated, potentially transitioning to monoclinic wairakite over longer time periods (>8 weeks). At all temperatures, we also observed that the reacted bentonite had reduced expandability due to the formation of zeolites and other phases in the clay fraction, as well as Na-K exchange and the transition of montmorillonite to illitic clays. While decreased swelling capacity of the bentonite matrix is not considered favorable for repository barrier performance, the formation of zeolite minerals (analcime and wairakite) with potential radionuclide uptake behavior in the bentonite buffer may present alternative pathways to immobilizing radionuclides.

Acknowledgments and Funding

The authors acknowledge funding for this project through the Department of Energy's Spent Fuel and Waste Disposition campaign. Los Alamos National Laboratory has assigned the number LA-UR-23-34101 to this manuscript. Sandia National Laboratories is a multimission laboratory managed and operated by National Technology & Engineering Solutions of Sandia, LLC, a wholly owned subsidiary of Honeywell International Inc., for the U.S. Department of Energy's National Nuclear Security Administration under contract DE-NA0003525. Sandia National Laboratories has assigned the number SAND2024-06886O to the text.

This paper describes objective technical results and analysis. Any subjective views or opinions that might be expressed in the paper do not necessarily represent the views of the U.S. Department of Energy or the United States Government. This is a technical paper that does not take into account the contractual limitations under the Standard Contract for Disposal of Spent Nuclear Fuel and/or High-Level Radioactive Waste (Standard Contract) (10 CFR Part 961). For example, under the provisions of the Standard Contract, DOE does not consider spent nuclear fuel in multi-assembly canisters to be an acceptable waste form, absent a mutually agreed-upon contract amendment. To the extent discussions or recommendations in this paper conflict with the provisions of the Standard Contract, the Standard Contract governs the obligations of the parties, and this paper in no manner supersedes, overrides, or amends the Standard Contract. This paper reflects technical work that could support future decision-making by DOE. No inferences should be drawn from this paper regarding future actions by DOE, which are limited both by the terms of the Standard Contract and a lack of Congressional appropriations for the Department to fulfill its obligations under the Nuclear Waste Policy Act, including licensing and construction of a spent nuclear fuel repository.

This article has been authored by an employee of National Technology & Engineering Solutions of Sandia, LLC, under Contract No. DE-NA0003525 with the U.S. Department of Energy (DOE). The employee owns all rights, title, and interest in and to the article and is solely responsible for its contents. The U.S. Government retains and the publisher, by accepting the article for publication, acknowledges that the U.S. Government retains a non-exclusive, paid-up, irrevocable, worldwide license to publish or reproduce the published form of this article or allow others to do so, for U.S. Government purposes. The DOE will provide public access to these results of federally sponsored research in accordance with the DOE Public Access Plan https://www.energy.gov/downloads/doe-public-access-plan (accessed on 20 November 2022).

References Cited

Alby, D., Charnay, C., Heran, M., Prelot, B., and Zajac, J. (2018) Recent developments in nanostructured inorganic materials for sorption of cesium and strontium: Synthesis and shaping, sorption capacity, mechanisms, and selectivity—A review. Journal of Hazardous Materials, 344, 511–530, https://doi.org/10.1016/j.jhazmat.2017.10.047.

Ames, L. Jr. (1960) The cation sieve properties of clinoptilolite. American Mineralogist, 45, 689–700.

——— (1966) Cation exchange properties of wairakite and analcime. American Mineralogist, 51, 903–909.

Aoki, M. and Minato, H. (1980) Lattice constants of wairakite as a function of chemical composition. American Mineralogist, 65, 1212–1216.

Apted, M.J. and Ahn, J. (2017) Geological Repository Systems for Safe Disposal of Spent Nuclear Fuels and Radioactive Waste, 802 p. Woodhead Publishing.

Azizi, S.N. and Yousefpour, M. (2011) Isomorphous substitution of iron and nickel into analcime zeolite. Zeitschrift für anorganische und allgemeine Chemie (ZAAC), 637, 759–765.

Bakatula, E.N., Mosai, A.K., and Tutu, H. (2015) Removal of uranium from aqueous solutions using ammonium-modified zeolite. South African Journal of Chemistry, 68, 165–171, https://doi.org/10.17159/0379-4350/2015/v68a23.

Bargar, K.E. and Beeson, M.H. (1981) Hydrothermal alteration in research drill hole Y-2, Lower Geyser Basin, Yellowstone National Park, Wyoming. American Mineralogist, 66, 473–490.

Bayliss, P. and Levinson, A.A. (1971) Low temperature hydrothermal synthesis from dolomite or calcite, quartz and kaolinite. Clays and Clay Minerals, 19(2), 109–114. https://doi.org/10.1346/CCMN.1971.0190207

Bethke, C.M., Farrell, B., and Yeakel, S. (2018) The Geochemist's Workbench Release 12, GWB Essentials Guide; Aqueous Solutions.

Bhalara, P.D., Punetha, D., and Balasubramanian, K. (2014) A review of potential remediation techniques for uranium (VI) ion retrieval from contaminated aqueous environment. Journal of Environmental Chemical Engineering, 2, 1621–1634, https://doi.org/10.1016/j.jece.2014.06.007.

Bildstein, O., Claret, F., and Frugier, P. (2019) RTM for waste repositories. Reviews in Mineralogy and Geochemistry, 85, 419–457, https://doi.org/10.2138/rmg.2019.85.14.

Blanc, P., Lassin, A., and Piantone, P. (2007) Thermoddem, version V1: 10: A database devoted to waste minerals. Orléans.

Campbell, L.S. and Davies, B. (1997) Experimental investigation of plant uptake of caesium from soils amended with clinoptilolite and calcium carbonate. Plant and Soil, 189, 65–74, https://doi.org/10.1023/A:1004223225189.

Cantrell, K. (1996) A permeable reactive wall composed of clinoptilolite for containment of Sr-90 in Hanford groundwater. American Nuclear Society, Inc.

Caporuscio, F.A., Palaich, S.E., Cheshire, M., and Jové Colón, C.F. (2017) Corrosion of copper and authigenic sulfide mineral growth in hydrothermal bentonite experiments. Journal of Nuclear Materials, 485, 137–146, https://doi.org/10.1016/j.jnucmat.2016.12.036.

Chermak, J. (1992) Low temperature experimental investigation of the effect of high pH NaOH solutions on the Opalinus Shale, Switzerland. Clays and Clay Minerals, 40, 650–658, https://doi.org/10.1346/CCMN.1992.0400604.

Cheshire, M.C., Caporuscio, F., Jové-Colón, C., and McCarney, M. (2013) Alteration of clinoptilolite into high-silica analcime within a bentonite barrier system under used nuclear fuel repository conditions. Proceedings of the 14th International High-Level Radioactive Waste Management (6893).

Cheshire, M.C., Caporuscio, F.A., Rearick, M.S., Jové-Colón, C., and McCarney, M.K. (2014) Bentonite evolution at elevated pressures and temperatures: An experimental study for generic nuclear repository designs. American Mineralogist, 99, 1662–1675, https://doi.org/10.2138/am.2014.4673.

Cheshire, M.C., Caporuscio, F.A., Jové-Colón, C., and Norskog, K.E. (2018) Fe-saponite growth on low-carbon and stainless steel in hydrothermal-bentonite experiments. Journal of Nuclear Materials, 511, 353–366, https://doi.org/10.1016/j.jnucmat.2018.09.038.

Chipera, S.J. and Apps, J.A. (2001) Geochemical stability of natural zeolites. Reviews in Mineralogy and Geochemistry, 45, 117–161, https://doi.org/10.2138/rmg.2001.45.3.

Chipera, S.J. and Bish, D.L. (2002) FULLPAT: A full-pattern quantitative analysis program for X-ray powder diffraction using measured and calculated patterns. Journal of Applied Crystallography, 35, 744–749, https://doi.org/10.1107/S0021889802017405.

Cho, M. and Liou, J. (1987) Prehnite-pumpellyite to greenschist fades transition in the Karmutsen metabasites, Vancouver Island, BC. Journal of Petrology, 28, 417–443, https://doi.org/10.1093/petrology/28.3.417.

Chung, F.H. (1974) Quantitative interpretation of X-ray diffraction patterns of mixtures. I. Matrix-flushing method for quantitative multicomponent analysis. Journal of Applied Crystallography, 7, 519–525, https://doi.org/10.1107/S0021889874010375.

Coombs, D.S. (1955) X-ray observations on wairakite and non-cubic analcime. Mineralogical Magazine and Journal of the Mineralogical Society, 30, 699–708, https://doi.org/10.1180/minmag.1955.030.230.03.

Cuadros, J. and Linares, J. (1996) Experimental kinetic study of the smectite-to-illite transformation. Geochimica et Cosmochimica Acta, 60, 439–453, https://doi.org/10.1016/0016-7037(95)00407-6.

Davis, M.E. and Lobo, R.F. (1992) Zeolite and molecular sieve synthesis. Chemistry of Materials, 4, 756–768, https://doi.org/10.1021/cm00022a005.

de la Villa, R.V., Cuevas, J., Ramírez, S., and Leguey, S. (2001) Zeolite formation during the alkaline reaction of bentonite. European Journal of Mineralogy, 13, 635–644, https://doi.org/10.1127/0935-1221/2001/0013-0635.

Deer, A., Howie, R., and Zussman, J. (2004) Rock Forming Minerals, Vol. 4B: Framework Silicates – Silica Minerals, Feldspathoids and the Zeolites. The Geological Society of London.

Dyer, A. (1988) An Introduction to Zeolite Molecular Sieves, 1st ed., 164 p. Wiley.

Eberl, D. and Hower, J. (1976) Kinetics of illite formation. Geological Society of America Bulletin, 87, 1326–1330, https://doi.org/10.1130/0016-7606(1976)87<1326:KOIF>2.0.CO;2.

Eberl, D., Velde, B., and McCormick, T. (1993) Synthesis of illite-smectite from smectite at earth surface temperatures and high pH. Clay Minerals, 28, 49–60, https://doi.org/10.1180/claymin.1993.028.1.06.

Fabian, M., Czompoly, O., Tolnai, I., and De Windt, L. (2023) Interactions between C-steel and blended cement in concrete under radwaste repository conditions at 80 °C. Scientific Reports, 13, 15372, https://doi.org/10.1038/s41598-023-42645-6.

Gaucher, E.C. and Blanc, P. (2006) Cement/clay interactions—a review: Experiments, natural analogues, and modeling. Waste Management, 26, 776–788, https://doi.org/10.1016/j.wasman.2006.01.027.

Grant, D., Skriba, M., and Saha, A.K. (1987) Removal of radioactive contaminants from West Valley waste streams using natural zeolites. Environmental Progress, 6, 104–109, https://doi.org/10.1002/ep.670060212.

Greenberg, H., Wen, J., and Buscheck, T. (2013) Scoping Thermal Analysis of Alternative Dual-Purpose Canister Disposal Concepts, 54 p. Lawrence Livermore National Lab.

Harada, K. and Nagashima, K. (1972) New data on the analcime–wairakite series. American Mineralogist, 57, 924–931.

Hardin, E., Bryan, C.R., Ilgen, A.G., Kalinina, E.A., Banerjee, K., Clarity, J., Howard, R., Jubin, R., Scaglione, J., and Perry, F. (2014) Investigations of Dual-purpose Canister Direct Disposal Feasibility (FY14), 214 p. Sandia National Lab.

Hardin, E., Hadgu, T., and Clayton, D.J. (2015) Cavern/Vault Disposal Concepts and Thermal Calculations for Direct Disposal of 37-PWR Size DPCs, 25 p. Sandia National Lab.

Hedin, A. (1997) Spent nuclear fuel—How dangerous is it? Svensk Kärnbränslehantering Aktiebolag (SKB) Report, 97–13.

Iijima, A. and Hay, R.L. (1968) Analcime composition in tuffs of the Green River Formation of Wyoming. American Mineralogist, 53, 184–200.

IMA (2008) IMA Database of Mineral Properties, https://rruff.info/ima/.

İnan, S. (2022) Inorganic ion exchangers for strontium removal from radioactive waste: A review. Journal of Radioanalytical and Nuclear Chemistry, 331, 1137–1154, https://doi.org/10.1007/s10967-022-08206-3.

International Zeolite Association (2023) Analcime Datasheet. International Zeolite Association. https://www.iza-online.org/natural/Datasheets/Analcime/Analcime.html.

Jiménez-Reyes, M., Almazán-Sánchez, P.T., and Solache-Ríos, M. (2021) Radioactive waste treatments by using zeolites. A short review. Journal of Environmental Radioactivity, 233, 106610, https://doi.org/10.1016/j.jenvrad.2021.106610.

Jove, C. and Hacker, B.R. (1997) Experimental investigation of laumontite → wairakite + H_2O: A model diagenetic reaction. American Mineralogist, 82, 781–789, https://doi.org/10.2138/am-1997-7-817.

Kabekkodu, S.N., Faber, J., and Fawcett, T. (2002) New Powder Diffraction File (PDF-4) in relational database format: Advantages and data-mining capabilities. Acta Crystallographica Section B, 58, 333–337, https://doi.org/10.1107/S0108768102002458.

Katsuki, K., Suzuki, H., Hasegawa, M., Heike, M., Hosomachi, N., Yamashita, Y., and Nakamura, Y. (2007) Effect of reaction temperature on Fe-Al analcime formation. Journal of Porous Materials, 14, 443–448, https://doi.org/10.1007/s10934-006-9038-6.

Kaufhold, S. and Dohrmann, R. (2016) Distinguishing between more and less suitable bentonites for storage of high-level radioactive waste. Clay Minerals, 51, 289–302, https://doi.org/10.1180/claymin.2016.051.2.14.

Kerrisk, J.F. (1983) Reaction-path calculations of groundwater chemistry and mineral formation at Rainier Mesa, Nevada, 24 p. Los Alamos National Lab.

Kersting, A., Zavarin, M., Zhao, P., Dai, Z., Carroll, S., Wang, Y., Miller, A., James, S., Reimus, P., and Zheng, L. (2012) Radionuclide interaction and

transport in representative geologic media. Used Fuel Disposition Campaign Milestone Report FCRD-UFD-2012-000154.
Kursten, B., Smailos, E., Azkarate, I., Werme, L., Smart, N., Marx, G., Cuñado, M., and Santarini, G. (2004) Corrosion evaluation of metallic HLW/spent fuel disposal containers-review. Conference: Prediction of Long Term Corrosion Behaviour in Nuclear Waste Systems. Eurocorr 2004, Volume I.
Liljenfeldt, H., Banerjee, K., Clarity, J.B., Scaglione, J., Jubin, R.T., Sobes, V., Howard, R.L., Hardin, E., Price, L., and Kalinina, E. (2017) Summary of Investigations on Technical Feasibility of Direct Disposal of Dual-Purpose Canisters, 117 p. Oak Ridge National Lab.
Liou, J. (1970) Synthesis and stability relations of wairakite, $CaAl_2Si_4O_{12}{\cdot}2H_2O$. Contributions to Mineralogy and Petrology, 27, 259–282, https://doi.org/10.1007/BF00389814.
Liou, J.G. (1971) Analcime Equilibria. Lithos, 4, 389–402.
Lothenbach, B., Bernard, E., and Mäder, U. (2017) Zeolite formation in the presence of cement hydrates and albite. Physics and Chemistry of the Earth Parts A/B/C, 99, 77–94, https://doi.org/10.1016/j.pce.2017.02.006.
Mallah, M.H., Soorchi, H., and Jooybari, T.F. (2012) Development of empirical equation for analcime in the treatment of nuclear waste. Annals of Nuclear Energy, 47, 140–145, https://doi.org/10.1016/j.anucene.2012.04.015.
Mills, M.M., Sanchez, A.C., Boisvert, L., Payne, C.B., Ho, T.A., and Wang, Y. (2023) Understanding smectite to illite transformation at elevated (>100° C) temperature: Effects of liquid/solid ratio, interlayer cation, solution chemistry and reaction time. Chemical Geology, 615, 121214, https://doi.org/10.1016/j.chemgeo.2022.121214.
Mimura, H., Ishihara, Y., and Akiba, K. (1991) Adsorption behavior of americium on zeolites. Journal of Nuclear Science and Technology, 28, 144–151.
MinDat (2024) MinDat Mineral Database and Mineralogical Reference Website. MinDat.org.
Misaelides, P. (2011) Application of natural zeolites in environmental remediation: A short review. Microporous and Mesoporous Materials, 144, 15–18, https://doi.org/10.1016/j.micromeso.2011.03.024.
Moore, D.M. and Reynolds, R.C. Jr. (1989) X-ray Diffraction and the Identification and Analysis of Clay Minerals, 352 p. Oxford University Press.
Mosser-Ruck, R., Pignatelli, I., Bourdelle, F., Abdelmoula, M., Barres, O., Guillaume, D., Charpentier, D., Rousset, D., Cathelineau, M., and Michau, N. (2016) Contribution of long-term hydrothermal experiments for understanding the smectite-to-chlorite conversion in geological environments. Contributions to Mineralogy and Petrology, 171, 1–21, https://doi.org/10.1007/s00410-016-1307-z.
Neuhoff, P.S. and Ruhl, L.S. (2006) Mechanisms and geochemical significance of Si-Al substitution in zeolite solid solutions. Chemical Geology, 225, 373–387, https://doi.org/10.1016/j.chemgeo.2005.08.029.
Neuhoff, P.S., Stebbins, J.F., and Bird, D.K. (2003) Si-Al disorder and solid solutions in analcime, chabazite, and wairakite. American Mineralogist, 88, 410–423, https://doi.org/10.2138/am-2003-2-317.
Neuhoff, P.S., Hovis, G.L., Balassone, G., and Stebbins, J.F. (2004) Thermodynamic properties of analcime solid solutions. American Journal of Science, 304, 21–66, https://doi.org/10.2475/ajs.304.1.21.
N s, B. (2020) Needs of countries with longer timescale for deep geological repository implementation. EPJ Nuclear Sciences & Technologies, 6, 22, https://doi.org/10.1051/epjn/2019042.
Ogihara, S. (1996) Diagenetic transformation of clinoptilolite to analcime in silicic tuffs of Hokkaido, Japan. Mineralium Deposita, 31, 548–553, https://doi.org/10.1007/BF00196135.
Oscarson, R.L. and Bargar, K.E. (1996) Electron microprobe analyses of zeolite minerals from Neogene volcanic rocks in the Breitenbush-Austin Hot Springs area. U.S. Geological Survey.
Passaglia, E. and Sheppard, R.A. (2001) The crystal chemistry of zeolites. Reviews in Mineralogy and Geochemistry, 45, 69–116, https://doi.org/10.2138/rmg.2001.45.2.
Pe-Piper, G. and Miller, L. (2002) Zeolite minerals from the north shore of the Minas Basin, Nova Scotia. Atlantic Geology, 38, 11–28.
Pearson, F., Arcos, D., Bath, A., Boisson, J., Fernandez, A., Gäbler, H., Gaucher, E., Gautschi, A., Griffault, L., and Hernán, P. (2003) Mont Terri Project—Geochemistry of Water in the Opalinus Clay Formation at the Mont Terri Rock Laboratory. Reports of the Federal Office for Water and Geology (FOWG) Geology Series No. 5.
Phillippo, M., Gvozdanovic, S., Gvozdanovic, D., Chesters, J.K., Paterson, E., and Mills, C.F. (1988) Reduction of radiocaesium absorption by sheep consuming feed contaminated with fallout from Chernobyl. The Veterinary Record, 122, 560–563, https://doi.org/10.1136/vr.122.23.560.
Pouchou, J. and Pichoir, F. (1985) "PAP"(ϕ-ρ-Z) procedure for improved quantitative microanalysis. In J.T. Armstrong, Ed., Microbeam Analysis, p. 104–106. San Francisco Press.
Pusch, R. (2009) Geological Storage of Highly Radioactive Waste: Current Concepts and Plans for Radioactive Waste Disposal, 398 p. Springer.
Pusch, R., Kasbohm, J., Knutsson, S., Yang, T., and Nguyen-Thanh, L. (2015) The role of smectite clay barriers for isolating high-level radioactive waste (HLW) in shallow and deep repositories. Procedia Earth and Planetary Science, 15, 680–687, https://doi.org/10.1016/j.proeps.2015.08.084.
Rabideau, A.J., Van Benschoten, J., Patel, A., and Bandilla, K. (2005) Performance assessment of a zeolite treatment wall for removing Sr-90 from groundwater. Journal of Contaminant Hydrology, 79, 1–24, https://doi.org/10.1016/j.jconhyd.2005.04.003.
Rajec, P., Macášek, F., and Misaelides, P. (1999) Sorption of heavy metals and radionuclides on zeolites and clays. Natural Microporous Materials in Environmental Technology, 353–363.
Sauer, K., Caporuscio, F., Rock, M., Cheshire, M., and Jové-Colón, C. (2020) Hydrothermal interaction of Wyoming bentonite and Opalinus clay. Clays and Clay Minerals, 68, 144–160, https://doi.org/10.1007/s42860-020-00068-8.
Savage, D. (2011) A review of analogues of alkaline alteration with regard to long-term barrier performance. Mineralogical Magazine, 75, 2401–2418, https://doi.org/10.1180/minmag.2011.075.4.2401.
Savage, D., Walker, C., Arthur, R., Rochelle, C., Oda, C., and Takase, H. (2007) Alteration of bentonite by hyperalkaline fluids: A review of the role of secondary minerals. Physics and Chemistry of the Earth Parts A/B/C, 32, 287–297, https://doi.org/10.1016/j.pce.2005.08.048.
Seki, Y. (1968) Synthesized wairakites: Their difference from natural wairakites. Chishitsugaku Zasshi, 74, 457–458, https://doi.org/10.5575/geosoc.74.457.
Seki, Y. and Oki, Y. (1969) Wairakite-analcime solid solutions from low-grade metamorphic rocks of the Tanzawa Mountains, Central Japan. Mineralogical Journal, 6, 36–45, https://doi.org/10.2465/minerj1953.6.36.
Sellin, P. and Leupin, O.X. (2013) The use of clay as an engineered barrier in radioactive-waste management—A review. Clays and Clay Minerals, 61, 477–498, https://doi.org/10.1346/CCMN.2013.0610601.
Seyfried, W., Janecky, D.R., Berndt, M.E., Ulmer, G., and Barnes, H. (1987) Rocking autoclaves for hydrothermal experiments II. The flexible reaction-cell system. Hydrothermal experimental techniques, 23.
Shushkov, D., Kotova, O., and Shuktomova, I. (2013) Removal of radionuclides by analcime-bearing rocks, 47, 012041. Presented at the IOP Conference Series: Materials Science and Engineering. IOP Publishing.
Sipos, P., Németh, T., and Máthé, Z. (2010) Preliminary results on the Co, Sr and Cs sorption properties of the analcime-containing rock type of the Boda Siltstone Formation. Central European Geology, 53, 67–78, https://doi.org/10.1556/CEuGeol.53.2010.1.4.
Smith, J. (1963) Structural classification of zeolites. Mineralogical Society of America, Special Papers, 1, 281–290.
rodo , J. (1980) Precise identification of illite/smectite interstratifications by X-ray powder diffraction. Clays and Clay Minerals, 28, 401–411, https://doi.org/10.1346/CCMN.1980.0280601.
Steiner, A. (1955) Wairakite, the calcium analogue of analcime, a new zeolite mineral. Mineralogical Magazine and Journal of the Mineralogical Society, 30, 691–698, https://doi.org/10.1180/minmag.1955.030.230.02.
Surdam, R.C. (1973) Low-grade metamorphism of tuffaceous rocks in the Karmutsen Group, Vancouver Island, British Columbia. Geological Society of America Bulletin, 84, 1911–1922, https://doi.org/10.1130/0016-7606(1973)84<1911:LMOTRI>2.0.CO;2.
Tahervand, S. and Jalali, M. (2017) Sorption and desorption of potentially toxic metals (Cd, Cu, Ni and Zn) by soil amended with bentonite, calcite and zeolite as a function of pH. Journal of Geochemical Exploration, 181, 148–159, https://doi.org/10.1016/j.gexplo.2017.07.005.
Tinseau, E., Bartier, D., Hassouta, L., Devol-Brown, I., and Stammose, D. (2006) Mineralogical characterization of the Tournemire argillite after in situ interaction with concretes. Waste Management, 26, 789–800, https://doi.org/10.1016/j.wasman.2006.01.024.
Verstricht, J. (2009) The ESDRED project: Engineering studies and demonstration of repository designs. Belgian Nuclear Research Center SCK-CEN.
Vieillard, P. (2010) A predictive model for the entropies and heat capacities of zeolites. European Journal of Mineralogy, 22, 823–836.
Vitali, F., Blanc, G., and Larque, P. (1995) Zeolite distribution in volcaniclastic deep-sea sediments from the Tonga Trench margin (SW Pacific). Clays and Clay Minerals, 43, 92–104, https://doi.org/10.1346/CCMN.1995.0430111.
Whitney, G. (1990) Role of water in the smectite-to-illite reaction. Clays and Clay Minerals, 38, 343–350, https://doi.org/10.1346/CCMN.1990.0380402.
Zandanel, A., Sauer, K.B., Rock, M., Caporuscio, F.A., Telfeyan, K., and Matteo, E.N. (2022) Impacts of crystalline host rock on repository barrier materials at 250° C: Hydrothermal Co-alteration of Wyoming bentonite and steel in the presence of Grimsel granodiorite. Minerals, 12, 1556, https://doi.org/10.3390/min12121556.

Manuscript received June 7, 2024
Manuscript accepted November 7, 2024
Accepted manuscript online November 19, 2024
Manuscript Handled by Lindsay J. McHenry

Endnotes:

[1]Deposit item AM-25-79490. Online Materials are free to all readers. Go online, via the table of contents or article view, and find the tab or link for supplemental materials.